Self-Standing, Conducting and Capacitive Biomimetic Hybrid Nanomembranes for Selective Molecular Ions Separation

Anna Puiggalí-Jou,[1,2] *Brenda G. Molina*,[1,2] *Maximilien Lopes-Rodrigues*,[1,2,3] *Catherine Michaux*,[3] *Eric A. Perpète*,[3] *David Zanuy*[1] *and Carlos Alemán*[1,2,4,*]

[1] Departament d'Enginyeria Química, EEBE, Universitat Politècnica de Catalunya, C/Eduard Maristany 10-14, Edif. I2, 08019, Barcelona, Spain.

[2] Barcelona Research Center for Multiscale Science and Engineering, EEBE, Universitat Politècnica de Catalunya, C/Eduard Maristany 10-14, Edif. C, 08019, Barcelona, Spain.

[3] Laboratoire de Chimie Physique des Biomolécules, Unité de Chimie Physique Théorique et Structurale (UCPTS), University of Namur, Rue de Bruxelles, 61, 5000 Namur, Belgium.

[4] Institute for Bioengineering of Catalonia (IBEC), The Barcelona Institute of Science and Technology, Baldiri Reixac 10-12, 08028 Barcelona Spain

[*] Corresponding author: carlos.aleman@upc.edu

ABSTRACT

Hybrid free-standing biomimetic materials are developed by integrating the VDAC36 β-barrel protein into robust and flexible three-layered polymer nanomembranes. The first and third layers are prepared by spin-coating a mixture of poly(lactic acid) (PLA) and poly(vinyl alcohol) (PVA). PVA nanofeatures are transformed into controlled nanoperforations by solvent-etching. The two nanoperforated PLA layers are separated by an electroactive layer, which is successfully electropolymerized by introducing a conducting sacrificial substrate under the first PLA nanosheet. Finally, the nanomaterial is consolidated by immobilizing the VDAC36 protein, active as an ion channel, into the nanoperforations of the upper layer. The integration of the protein causes a significant reduction of the material resistance, which decreases from 21.9 to 3.9 $k\Omega \cdot cm^2$. Electrochemical impedance spectroscopy studies using inorganic ions and molecular metabolites (*i.e.* L-lysine and ATP) not only reveal that the hybrid films behave as electrochemical supercapacitors but also indicate the most appropriated conditions to obtain selective response against molecular ions as a function of their charge. The combination of polymers and proteins is promising for the development of new devices for engineering, biotechnological and biomedical applications.

INTRODUCTION

Hybrid biomimetic membranes take advantage of biomolecules, which have gained excellence on their specificity and efficiency during millions of years, and also the benefits of artificial materials that load the purified biological molecules and provide technological properties, such as robustness, scalability and suitable nanofeatures to confine the biomolecules.[1-5] Molecular sensing, water purification and desalination, drug delivery and DNA sequencing are some striking applications of these 2D devices.

Porins are a class of outer membrane proteins (OMPs), which consist of β-barrel channels and are located in gram-negative bacteria and mitochondria.[6] β-Barrels are typically employed for the fabrication of hybrid biomimetic membranes,[7-11] amid other biomolecules and materials that have also attracted interest.[12-16] From the perspective of the employed materials, the approaches used to modify artificial membranes, which can be free-standing or tethered onto solid supports, with biomolecules are those based on the utilization of amphiphilic copolymers and nanostructured polymers.

The latter approach was successfully followed to embed an OMP, namely Omp2a,[17] in conducting polymer (CP) films made of poly(*N*-methylpyrrole) (PNMPy) supported on rigid stainless-steel electrodes.[9] Electrochemical impedance spectroscopy (EIS) measures showed that PNMPy/Omp2a preferentially promotes the passive transport of K^+ in solutions with relatively high ionic concentrations. Later, self-standing poly(lactic acid) (PLA) nanofilms were used as support for the Omp2a protein.[10] These films, which were prepared by spin-coating an immiscible mixture of poly(vinyl alcohol) (PVA) and PLA,[18] had nanoperforations (diameter: 51±22 nm) resulting from the combination of nanophase segregation processes and selective solvent etching. EIS assays evidenced that, with respect to nanoperforated PLA (npPLA) nanofilms without

protein, those loaded with the protein showed enhanced conductivity and selectivity against some ions.[19]

In a recent study, we reported a new approach for preparing free-standing films that combines the mechanical strength and flexibility of processed npPLA nanosheets with the electrochemical response of anodically polymerized CPs.[20] More specifically, 5-layered membranes made of three npPLA layers separated by two anodically polymerized poly(3,4-ethylenedioxythiophene) (PEDOT) layers were prepared and used as Faradaic motors able to push a huge amount of mass. More recently, we modified this approach by introducing the polymerization of 3-dodecylthiophene.[21] The dodecyl chains allowed us to incorporate an amphiphilic environment similar to that offered by lipids to mimic favorable environment for OMPs immobilization. However, we observed that, although poly(3-dodecylthiophene) slightly enhanced the integration of the OMP, the conduction pathways were more effective with PEDOT.

In this study we synergistically join such smart strategy to the functionality of Voltage Dependent Anion Channels (VDACs), which are porins found in the outer mitochondrial membrane of all eukaryotic cells,[21] to obtain biomimetic and free-standing hybrid films able to respond to molecular ions. The function of VDACs is associated to the permeability of the mitochondria, regulating the diffusion of metabolites.[22,23] Specifically, this work focusses on the utilization of VDAC from *Solanum tuberosum*, a plant (potato) model organism, hereafter named VDAC36,[24] to obtain free-standing multilayered hybrid films responsive to molecular ions. As the diameter of the VDAC36 channel is around twice that of previously used Omp2a (*i.e.* 2.0 vs 1.2 nm),[21] the former is more suitable for the diffusion of molecular ions than the latter.[25] In addition, VDACs are able to switch from an open state (high conductance) to a closed state (low conductance) depending on the environmental conditions, being

possible to modulate its diffusion activity. Consequently, we have examined the response of the developed films as a function of the charge of the molecular ion, the concentration of the molecular ion and the state of VDAC.

The experimental methods are provided in Electronic Supporting Information (ESI), and this work is organized as follows. First, we present a brief description of the approach followed for the preparation of the functionalized 3-layered films. The next two sub-sections discuss the morphology of the prepared films, as well as the chemical and structural characterization of the immobilized VDAC36 protein. The electrochemical response of VDAC36-functionalized 3-layered films is analyzed using electrochemical impedance EIS. After this, the response of the prepared films against molecular metabolites is investigated as a function of the charge and the open/closed state of the protein channel. Conclusions are outlined in the last section. Overall, this work shows that npPLA/PEDOT/npPLA/VDAC free-standing films are biomimetic, exhibit low electrical resistance, behave as a supercapacitor and respond selectively against solutions with low concentration of molecular metabolites.

RESULTS AND DISCUSSION

Preparation of VDAC36-functionalized films

In a recent study, self-standing 5-layered films were prepared and used as Faradaic motors for applications as artificial muscles.[20] Nanoindentation studies showed that the elastic modulus of films bearing three npPLA layers is 3.4 GPa. However, the mechanical requirements of artificial muscles are not necessary in this work since huge actuation strains will not be applied. Consequently, simple 3-layered films have been considered to develop biomimetic membranes. More specifically, robust, flexible and manageable free-standing films made of two npPLA layers separated by an

electrochemically polymerized PEDOT layer were obtained using the procedure illustrated by Figure 1a.

In brief, a poly(3,4-ethylenedioxythiophene): poly(styrenesulfonate) (PEDOT:PSS) film of 173 ± 19 nm in thickness was prepared as sacrificial layer by spin-coating a commercial water dispersion onto a steel electrode (Figure 1a-1). Then, a PLA:PVA layer was deposited onto the PEDOT:PSS film by spin-coating a PLA:PVA mixture in hexafluoroisopropanol (HFIP). (Figure 1a-2). As PLA and PVA are immiscible polymers, the resulting PLA:PVA layer displayed a phase segregation with the formation of PVA domains with dimensions similar to the entire film thickness (Figure 1a-3),[26] which is 135±18 nm. Nanofeatures converted into nanoperforations by selective solvent etching (Figure 1a-4), and the thickness of the resulting npPLA layer was 114 ± 11 nm. Nanoperforations in the PLA nano-layer were responsible for the successful anodic polymerization of PEDOT (Figure 1a-5), allowing the monomer molecules to cross the entire thickness and reach the semiconducting PEDOT:PSS layer. For this purpose, the steel electrode coated with PEDOT:PSS and npPLA was moved to an electrochemical cell, containing the monomer, and used as working electrode. The electropolymerization was performed adjusting the polymerization charge to 90 mC/cm^2. The PEDOT:PSS layer allowed the immobilization of the polymerized PEDOT chains, forming a very cohesive system with the npPLA layer. The PEDOT layer exhibited a thickness of 765±81 nm. Finally, the PEDOT layer was covered with a new nano-layer of npPLA of 167±31 nm in thickness, which was obtained as previously described (Figure 1a-6,7,8). Experimental details and operational conditions are described in the Supporting Information.

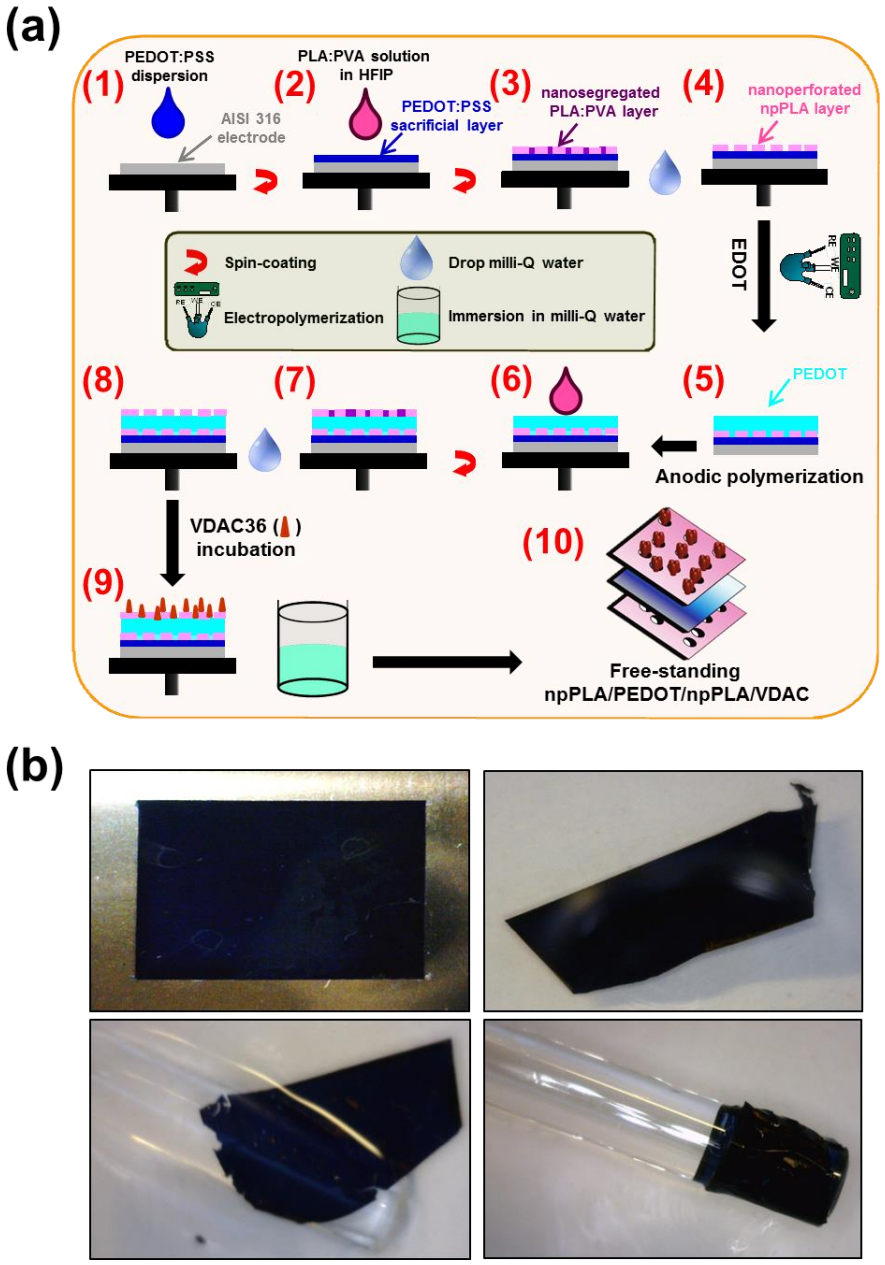

Figure 1. (a) Scheme illustrating the preparation of npPLA/PEDOT/npPLA/VDAC free-standing biomimetic films. The (1)-to-(10) steps are described in the text. Experimental details and operational conditions are provided in the Supporting Information. (b) Photographs showing the robustness and conformability of free standing npPLA/PEDOT/npPLA/VDAC films.

The immobilization of protein was found to be 32% higher when 3-dodecylthiophene was included in the CP layer due to the lipophilic environment created by the dodecyl side chains, which interact more favourably with the outside facing part of the VDAC36

β-barrel.[21] However, the π-conjugation and electrochemical activity are higher in PEDOT than in poly(3-methylthiophene) and in 3,4-ethylenedioxythiophene/3-methythiophene copolymers due to restrictions imposed by the cyclic substituent and the electron-donating effects of the oxygen atoms.[27] As in this work we are focused on the electrochemical response of films functionalized with the protein, the priority given to the intrinsic properties of the film was higher than to the amount of immobilized protein. Accordingly, the supported npPLA/PEDOT/npPLA 3-layered film, with a thickness of *ca.* 1.2 μm, was incubated with a VDAC36 solution additionally containing sodium dodecyl sulphate (SDS) and 2-methyl-2,4-pentanediol (MPD) for protein reconstitution. (Figure 1a-9). The successful immobilization of the protein onto the surface of the 3-layered film was proved by laser scanning confocal microscopy (see next section). Detachment of 3-layered films from steel substrates was achieved by selective elimination of the thin sacrificial layer (Figure 1a-10). Although PEDOT:PSS is not soluble in water, it forms a colloidal dispersion. After immersion into milli-Q water for 12 h, films were detached from the steel substrate and easily recovered with fine-point tweezers. The resulting npPLA/PEDOT/npPLA/VDAC free-standing films, which do not deteriorate during such process, are 1.05 μm in thickness and shows excellent robustness and conformability, as is evidenced by Figure 1b.

Morphological characterization of VDAC36-functionalized films

Figures 2a shows atomic force microscopy (AFM) images of the first spin-coated PLA:PVA layer (see additional images in Figure S1a). Phase contrast images evidence the presence of nanofeatures, consisting of separated PVA rounded-shape domains within the PLA matrix (lighter and darker contrast, respectively). The transformation of nanofeatures into nanopores occurred after PVA water-etching (Figures 2b and S1b).

The abundance and uniform distribution of the nanoperforations in the npPLA layer, which are 89 ± 14 nm in diameter, was confirmed by scanning electron microscopy (SEM; Figure 2c).

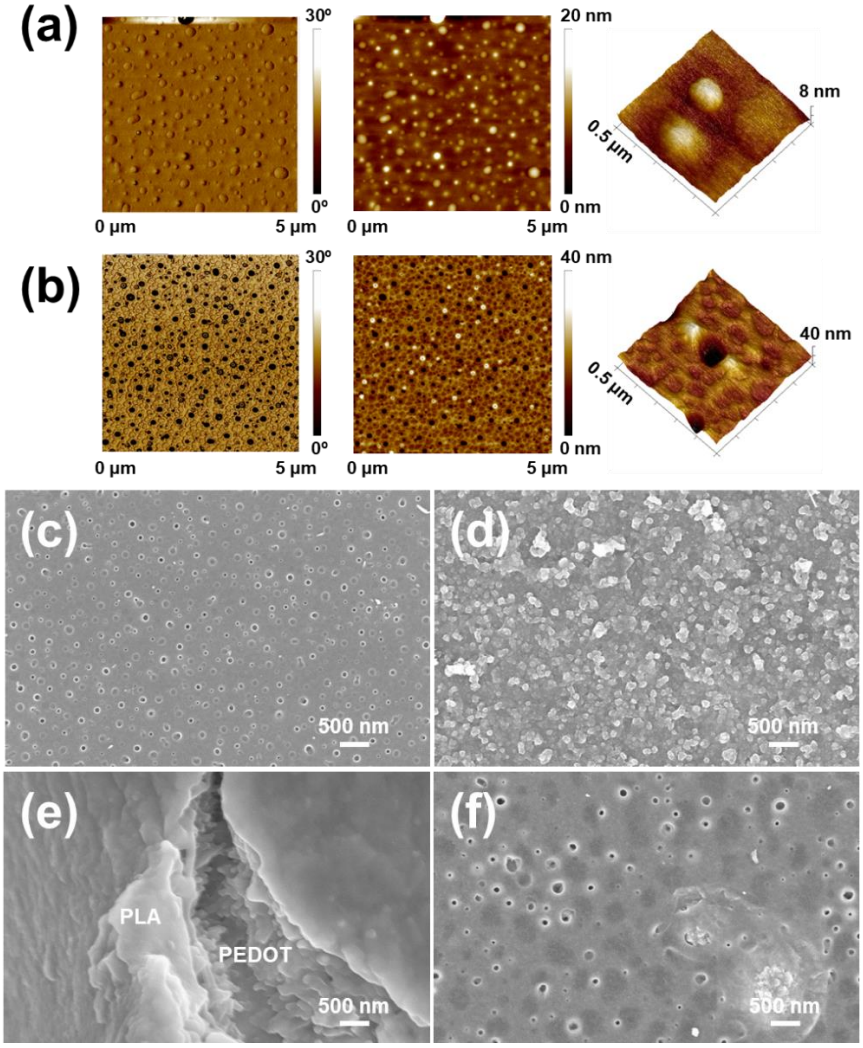

Figure 2. AFM phase (5 × 5 µm^2) and topographic (5 × 5 µm^2 and 0.5 × 0.5 µm^2) images of (a) PLA:PVA and (b) npPLA films (additional 10 × 10 µm^2 images are displayed in Figure S1). Representative high resolution SEM micrograph of: (c) the first npPLA layer, (d) the intermediate PEDOT layer, (e) the two sides of an intentionally scratched npPLA/PEDOT 2-layered film, and (f) the upper layer of the npPLA/PEDOT/npPLA 3-layered film.

On the one hand, the intermediate PEDOT layer, which exhibits the typical globular morphology (Figure 2d), was completely adhered to the first npPLA layer. The

cohesion between such npPLA and PEDOT layers is reflected in Figure 2e, which displays layers in an intentionally scratched film. On the other hand, the diameter of the nanoperforations in the second npPLA layer, 137 ± 25 nm, was greater than in the first layer (Figure 2f), evidencing that the PEDOT layer behaves as a mold in the spin-coating process.

SEM micrographs of npPLA/PEDOT/npPLA films incubated in both protein and blank solutions (Figure S2) allowed the identification of superficial SDS crystals, which frequently form from SDS micellar solutions.[28] As a result of its low tendency to associate into large hierarchical structures (*i.e.* cross-linking experiments showed the formation of dimers and tetramers only[25]), VDAC36 protein cannot be distinguished at the surface. However, visualization of the intrinsic protein fluorescence by confocal microscopy demonstrated the successful incorporation of VDAC36. Figure 3a-b compares the bright field images, the fluorescence images and the merged images recorded for 3-layered films before and after protein incubation, enabling the identification of the Tyr and the Trp of VDAC36 in npPLA/PEDOT/npPLA/VDAC by the fluorescence at 303 and 354 nm, respectively. Apparently, the protein is homogeneously immobilized over the entire surface, without preferential positions. This observation was corroborated by topographic and phase AFM images (Figure S3). Comparison of the images recorded for npPLA/PEDOT/npPLA films before and after incubation with VDAC36 evidenced that the protein was not only confined inside and around the nanopores of the npPLA layer but also adsorbed onto its electrochemically inactive surface. While only the protein immobilized in the pores is expected to contribute to the transport of molecular ions, regulation of the adsorption process to avoid the immobilization onto the surface is, unfortunately, a very difficult task.

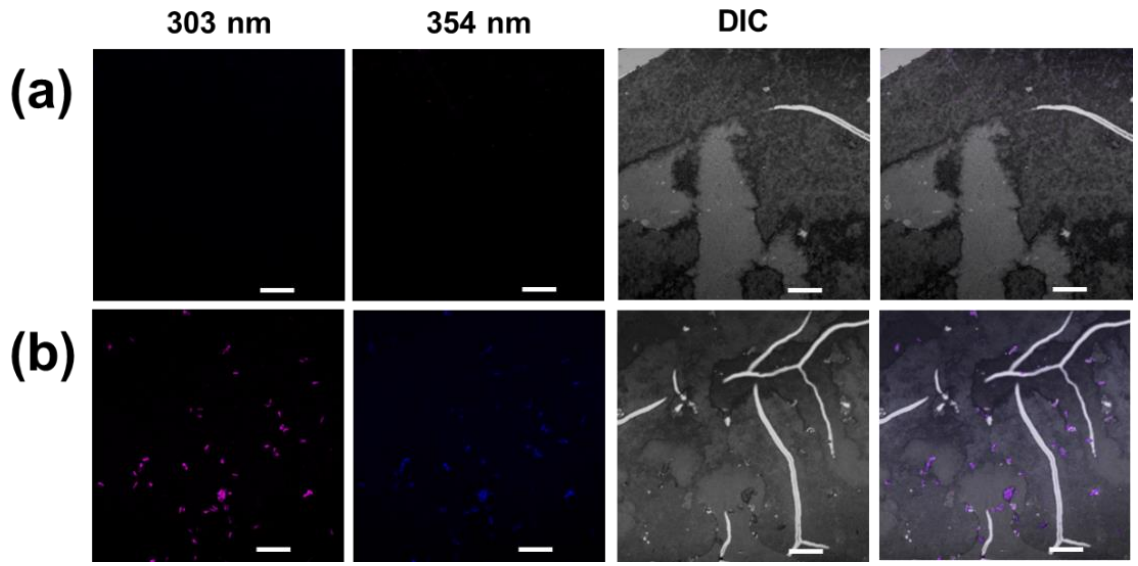

Figure 3. Confocal microscopy images of (a) npPLA/PEDOT/npPLA and (b) npPLA/PEDOT/npPLA/VDAC. The panels at the first and second columns correspond to the fluorescence images at different excitation/emission wavelengths for Tyr (303 nm) and Trp (354 nm), the panel at the third column shows the bright field images (DIC), and the panel at the right displays the merged images. Scale bar: 10 μm.

Characterization of the immobilized VDAC36 protein

Further characterization by XPS, contact angle measures, FTIR spectroscopy and CD unambiguously confirmed the immobilization of the protein. The atomic compositions of npPLA/PEDOT/npPLA and npPLA/PEDOT/npPLA/VDAC, as obtained by XPS, are compared in Table 1. The penetration of X-ray radiation using the conditions described in Methods section is expected to be ~10 nm, even though in this case the penetration is not accurately known due to the nanoperforations in the upper layer. The content of N 1s, which is undetectable for npPLA/PEDOT/npPLA, is 0.19% for npPLA/PEDOT/npPLA/VDAC. This feature, together with the increment of O 1s content, supports the presence of the protein.

Figure 4a compares the FTIR spectra from 890 to 1790 cm^{-1} of several films after detachment. Although the side chain bands of charged amino residues at ~1631 and

~1755 cm^{-1} are not identified because of the overlap with the bands associated to the thiophene ring (C=C and C–C stretching) of PEDOT,[29] it is possible from the typical amide band to unambiguously conclude that VDAC36 has been successfully immobilized. Indeed, the amide III and II vibrational modes of the protein, which arise from the coupling between the N−H in-plane bending and C−N stretching modes, are clearly recognizable at 1230 and 1514 cm^{-1}, respectively. The incorporation of the OMP is also supported by the peak at 970 cm^{-1}, which is not detected in the spectrum of npPLA/PEDOT/npPLA and has been attributed to the C–N stretching vibration in proteins.[30]

Table 1. Atomic percent composition obtained by XPS for the studied 3-layered films.

	C 1s	N 1s	O 1s	S 2p
npPLA/PEDOT/npPLA	72.01	0.00	27.88	0.11
npPLA/PEDOT/npPLA/VDAC	70.87	0.19	28.88	0.06

The immobilized protein not only remained within the free-standing 3-layered film, as proved by FTIR spectroscopy (Figure 4a), but it also preserved its β-barrel structure. Figure 4b compares the CD spectra recorded for VDAC36 in four different conditions: (i) unfolded (negative control); (ii) refolded; (iii) after immobilization onto the supported 3-layered film; and (iv) after detachment of the free-standing film. All spectra, with the exception of the unfolded protein, exhibit a broad minimum at 218-220 nm that is typically associated with β-stranded proteins.[31] The spectrum of the unfolded protein reflects the structural modifications associated with the conformational lost.

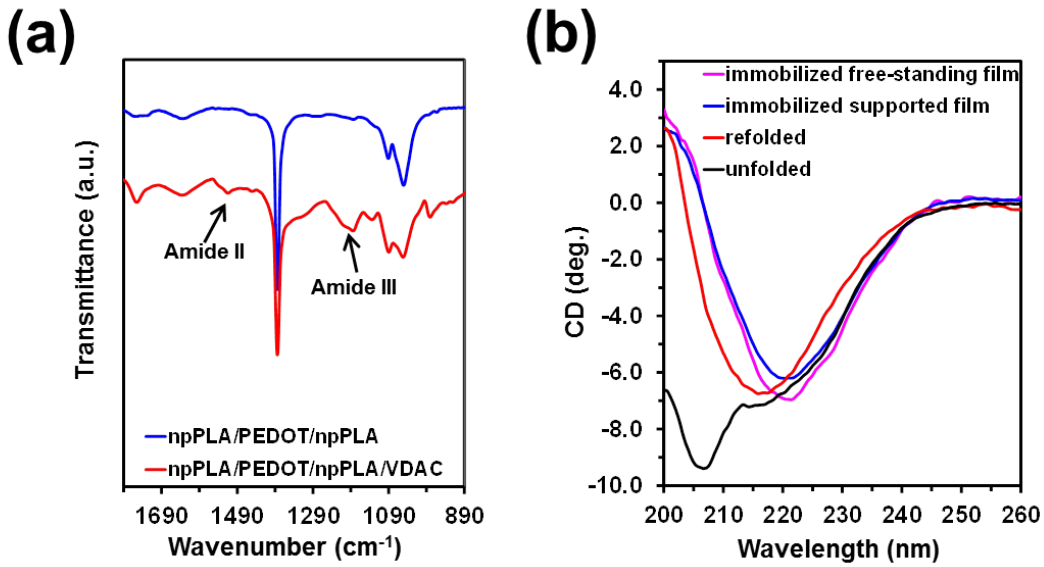

Figure 4. (a) FTIR spectra of 3-layered free standing films. (b) CD spectra for the VDAC36 protein: unfolded, refolded, after immobilization onto supported 3-layered films and after detachment of the 3-layered film from the steel substrate.

The contact angles (Θ) measured in water (Figure S4) also provided indirect evidences of the successful immobilization of VDAC36. The wettability of npPLA/PEDOT/npPLA (Θ=61°±7°) significantly increased upon the incorporation of the protein (Θ=41°±10°), which has been attributed to the effect of the hydrophilic residues found in the loops connecting the β-strands of the protein or inside the central pore.

Electrochemical response of non-functionalized and VDAC36-functionalized films

EIS studies were conducted on npPLA/PEDOT/npPLA and npPLA/PEDOT/npPLA/VDAC to monitor the changes in resistance and capacitance caused by the 3-layered configuration containing both npPLA and PEDOT with respect to simple films with only one of such components. The ion transport was evaluated by

measuring the impedance for frequencies ranging from 10^{-2} to 10^{5} Hz, using a 0.5 M NaCl solution and steel electrodes. Figure 5a-b displays the recorded Nyquist and Bode plots. The EECs used to fit the experimental data and the corresponding parameters are sketched in Figure 5c, where R_S is the electrolyte resistance and R_p represents the ability of the films to impede ion transport at the interface between the electrolyte and the film (*i.e.* the resistance of the film). The EECs also include double layer capacitances from both the 3-layered film and the steel electrode (CPE_{3L} and CPE_{st}, respectively) and a Warburg impedance element (W), corresponding to the diffusion of water molecules. In the case of npPLA/PEDOT/npPLA/VDAC, both R_p and CPE_{3L} include the overall contribution of the VDAC36-integrated interface. Both CPE_{3L} and CPE_{st} were modelled using a constant phase element (CPE). The percentage error associated to each circuit element was lower than 5% in virtually all cases.

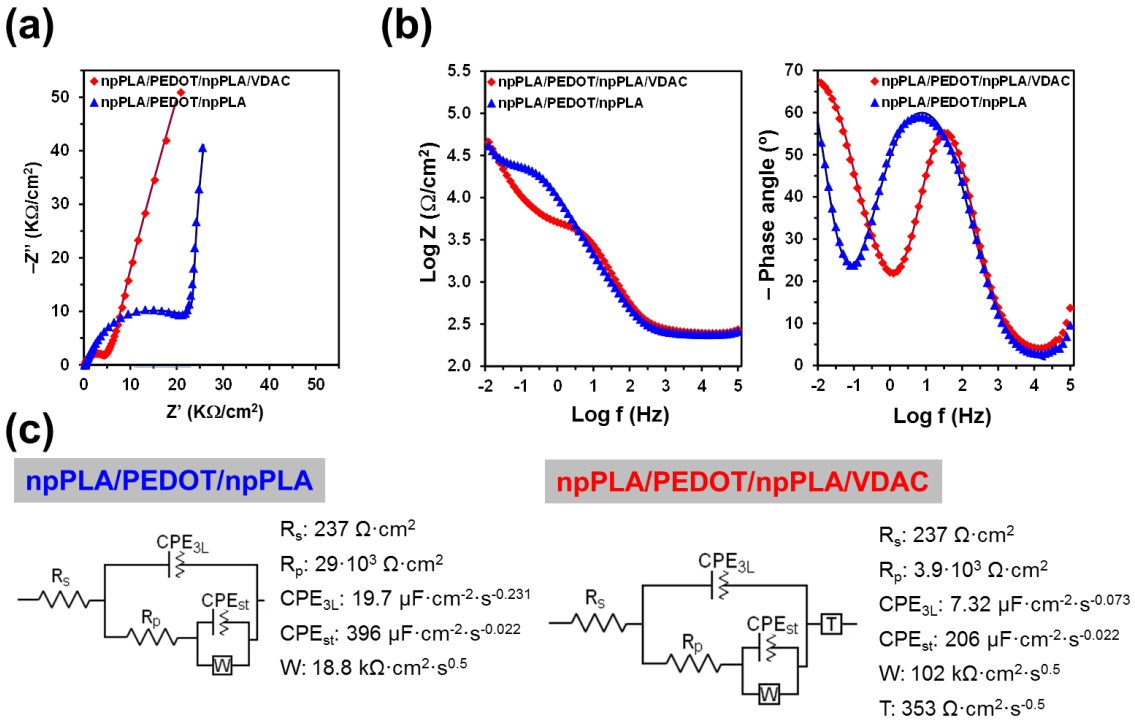

Figure 5. (a) Nyquist and (b) Bode plots in a 0.5 M NaCl aqueous solution and (c) EECs used for fitting experimental data recorded for npPLA/PEDOT/npPLA and npPLA/PEDOT/npPLA/VDAC. In (a,b) Symbols correspond to experimental data, while curves are fitted according to EEC.

The R_p of the 3-layered film functionalized with VDAC36 is one order of magnitude lower than for the film without protein (*i.e.* 3.9 and 21.9 $k\Omega \cdot cm^2$, respectively). Interestingly, the resistance of the npPLA/PEDOT/npPLA/VDAC film is very similar to that observed for the PPy/Omp2a film (1.3 $k\Omega \cdot cm^2$),[9] though the amount of CP contained was significantly higher. Similarly, the resistance reported for Omp2a protein supported onto lipid bilayers, which exhibited much less mechanical strength than 3-layered films, was of 3.7 $k\Omega \cdot cm^2$.[19] These results confirm that npPLA/PEDOT/npPLA/VDAC films behave as smart biomimetic membranes fulfilling the self-standing and mechanical integrity requirements of many applications in different areas of the biomedical field, such as nanofluidics, biosensing and energy conversion.

In addition to the heterogeneous characteristics of the electrode surface (*i.e.* roughness, porosity, reactivity), the CPE impedance is related to non-uniform diffusion across the interface. Accordingly, CPE is expressed as $[Q \cdot (j\omega)^n]^{-1}$, representing an ideal capacitor (n = 1), a pure resistor (n = 0) or a diffusion process (n = 0.5). For films without and with VDAC36, the value of n obtained for the CPE associated to CPE_{3L} is respectively 0.769 and 0.927, reflecting that the protein significantly improves the capacitive behaviour of the film. The well-known supercapacitive (*i.e.* electrochemically capacitive) response of PEDOT is typically attributed to its ability to promote series of fast and reversible redox reactions.[32,33] Our results show that the integration of the protein enhances this behaviour. This change is justified by the addition of the bounded Warburg diffusion impedance (T) element, which is characteristic of films containing a fixed amount of electroactive material (*i.e.* films of finite thickness). The addition of T, which is usually related to the diffusion resistance

of ions in doped electrodes of batteries and supercapacitors,[32,35,36] indicates that VDAC36 induces a fast transfer (and a subsequent adsorption) of electrolytes on the surface of the film. This leads to an increased CPE_{3L}, as demonstrated by the EEC parameters (Figure 5c), indicating that npPLA/PEDOT/npPLA/VDAC films are potential candidates for the fabrication of bio-supercapacitors and -batteries for bioelectronics and bionics.

Electrochemical response against molecular metabolites

In general, VDACs are known to regulate the diffusion of inorganic ions, such as NaCl and KCl, and metabolites such as nicotinamide adenine dinucleotide hydrogen (NADH) and adenosine triphosphate (ATP), through the outer mitochondrial membrane of eukaryotic cells.[22,37] At zero or low voltages, the channel of VDACs is open and exhibits a low resistance, which is consistent with a persistent flow of ions and/or metabolites crossing the membrane through it. At high voltages, the channel switches to partially closed states and the resistance increases, reflecting a reduction in the permeability to ions and metabolites.[37-39] Furthermore, in the open state there is a slight preference towards anions over cations, while the opposite selectivity is proposed for the partially closed state. How these effects are tuned by the salt or metabolite concentration is still a matter of scientific discussion.[40-42]

In this work, the response of npPLA/PEDOT/npPLA/VDAC towards molecular ions was examined using EIS. For this purpose, the impedance response of functionalized 3-layered films was evaluated considering 10, 50, 100 and 500 mM solutions of adenosine triphosphate (ATP) and L-lysine. Furthermore, the effect of the channel state was considered using unfolded (partially closed state) and folded (open state) proteins for the functionalization of the 3-layered films. More specifically, films functionalized with

unfolded VDAC36 (hereafter VDAC-u), were obtained by immobilizing the protein as purified, while films functionalized with folded VDAC36 (VDAC-f) involved the immobilization of the protein in a reconstituting environment with SDS and MPD, as is described above and is detailed in Methods section (ESI).

Nyquist plots obtained using 10 and 500 mM ATP and L-lysine solutions are displayed in Figure 6a, while those recorded for 50 and 100 mM solutions are shown in Figure S5. In order to facilitate the comparison between inorganic ions and molecular metabolites, results obtained using NaCl solutions with identical concentrations are included in Figures 6 and S5. In all cases, Nyquist plots, which represents the real part of the impedance against the imaginary part, shows a semicircle. As it can be seen, the diameter of the semicircle, which corresponds to the charge transfer resistance (R_p) at the film/electrolyte interface, depends not only on the charge of the metabolite but also on the state of the channel. The R_p values measured for the npPLA/PEDOT/npPLA/VDAC(f) and npPLA/PEDOT/npPLA/VDAC(u) films in the different solutions are compared in Figure 6b and Table S1.

As shown by the results, the R_p is much higher for L-lysine solutions than for ATP solutions, independently of the concentration and the state of the channel. Indeed, the difference between the R_p values obtained for solutions of these molecular metabolites at identical concentrations, $\Delta R_{p/Lys\text{-}ATP} = R_p(\text{L-lysine}) - R_p(\text{ATP})$, rapidly decreases with increasing metabolites concentration. For example, the value of $\Delta R_{p/Lys\text{-}ATP}$ found for npPLA/PEDOT/npPLA/VDAC(f) is 11622, 1384, 511 and 192 Ω for 10, 50, 100 and 500 mM solutions, respectively (Table S1). This variation indicates that the preference of VDAC36 towards anions is very pronounced at low metabolite concentrations, becoming only slight higher at the greatest metabolite concentration. Comparison with the $\Delta R_{p/Lys\text{-}ATP}$ values measured for npPLA/PEDOT/npPLA/VDAC(u) (6230, 1206, 495

and 125 Ω for 10, 50, 100 and 500 mM solutions, respectively) evidences that the state of the channel is only relevant for low concentrations, as the behaviour of films functionalized with folded and unfolded VDAC36 is similar for concentrations higher than 50 mM (Table S1).

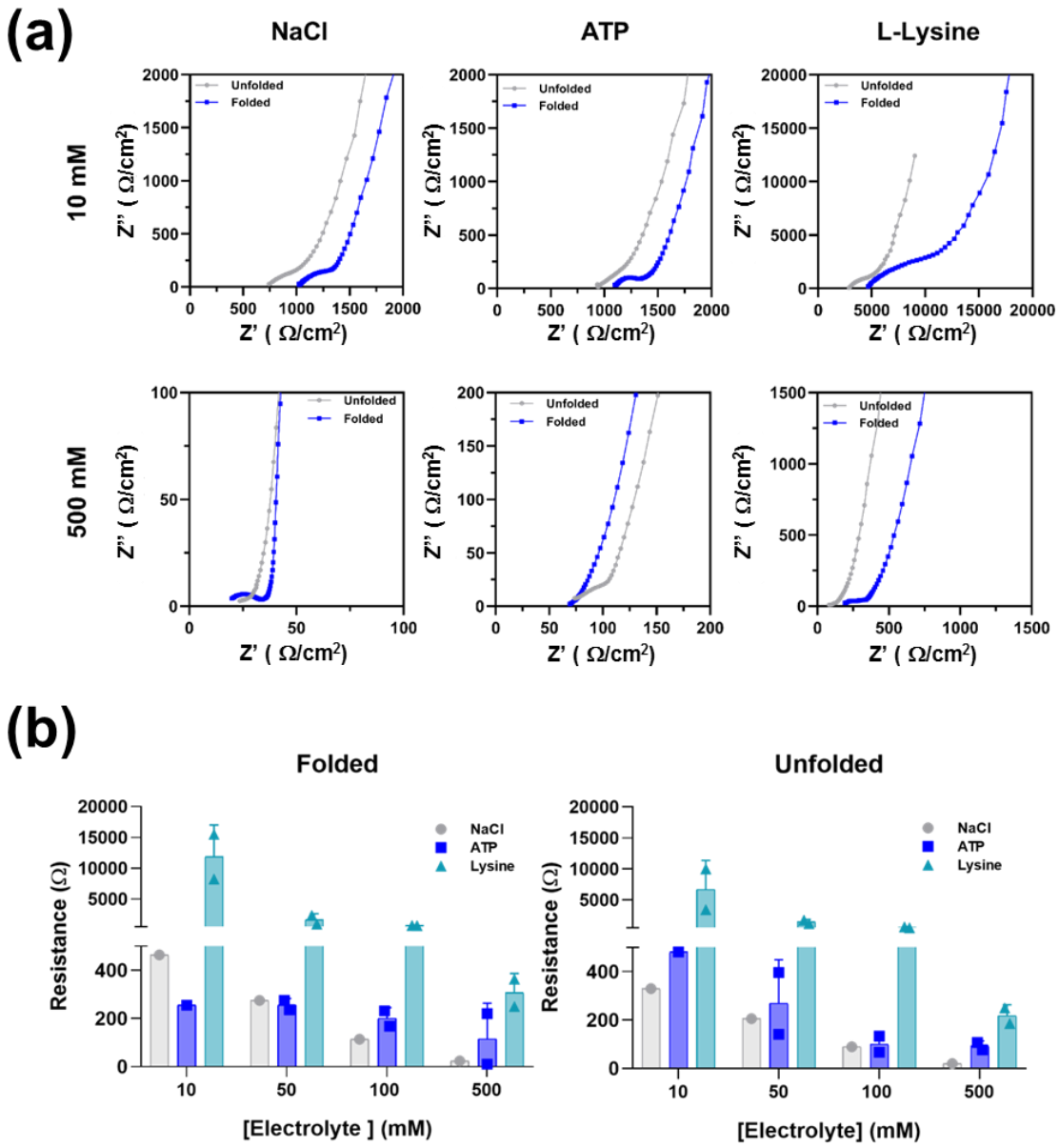

Figure 6. (a) Nyquist plots in a 10 mM (top) and 500 mM (down) NaCl, ATP and L-lysine aqueous solution for npPLA/PEDOT/npPLA/VDAC(f) (folded) and npPLA/PEDOT/npPLA/VDAC(u) (unfolded). The Nyquist plots obtained with 50 and 100 mM electrolyte solutions are shown in Figure S5. (b) R_p values measured for the npPLA/PEDOT/npPLA/VDAC(f) (left) and npPLA/PEDOT/npPLA/VDAC(u) (right) films in the different electrolyte solutions.

The dependence of the response of both npPLA/PEDOT/npPLA/VDAC(f) and npPLA/PEDOT/npPLA/VDAC(u) on the metabolite concentration has been attributed to the distribution of fixed charges inside the VDAC36 channel, which creates an electric field that determines the preference of the protein for ATP over Lys at low metabolite concentration. Thus, experimental $\Delta R_{p/Lys\text{-}ATP}$ values indicate that ATP molecules are more frequent inside VDAC36 protein, crossing its pore more frequently than Lys molecules. Increasing the metabolite concentration in the medium is expected to result in a higher concentration of ions in the VDAC36 wide pore. However, this event induces a large electrostatic screening of the charged residues, which is likely to be facilitated by the large pore size of VDAC36, promoting a less ATP selective channel. Thus, the channel becomes electrically neutral due to the screening of its charges and, consequently, the electric field responsible of the ATP attraction and Lys repulsion at low concentrations disappears.

Moreover, the analysis of the R_p values obtained using ATP solutions indicates that for each studied concentration the resistance is slightly lower for films functionalized with VDAC36(f) than for those with VAD36(u). However, the difference between the two systems, $\Delta R_{p/ATP(u\text{-}f)}$ = R_p[film with VDAC36(u)] – R_p[film with VDAC36(f)], decreases with increasing ATP concentration. For example, $\Delta R_{p/ATP(u\text{-}f)}$ was 226, 160, 35 and 98 Ω for 10, 50, 100 and 500 mM ATP solutions, respectively (Table S1). These figures indicate that the influence of the channel state on the regulation of the molecular anions flow decreases with increasing concentration. We could not detect this effect for L-lysine.

Finally, the results acquired for the npPLA/PEDOT/npPLA/VDAC(f) using NaCl and ATP solutions indicate that the performance of the membrane depends on the

concentration. The resistance is lower for ATP than for Cl^- with $\Delta R_{p/NaCl\text{-}ATP} = R_p(NaCl) - R_p(ATP) = 209\ \Omega$, while the difference is practically zero for 50 mM. On the contrary, $\Delta R_{p/NaCl\text{-}ATP}$ is slightly lower for Cl^- than for ATP for concentrations of 100 and 500 mM (*i.e.* 86 and 90 Ω, respectively). As expected and due to the steric hindrance associated to partially closed state, the diffusion of atomic anion in npPLA/PEDOT/npPLA/VDAC(u) films is favored with respect to the molecular anion .

CONCLUSIONS

In summary, we have established a methodology for the functional incorporation of porins in self-supported, stable, size-adaptable, conducting polymeric films made of two nanoperforated PLA layers separated by an intermediate PEDOT layer, which is produced by electrochemical polymerization. The immobilized protein preserves its β-barrel structure and increases the surface wettability of the film. The latter is particularly relevant for biotechnological and biomedical applications, in which aqueous environments are the most usual. This unprecedented combination of properties is accompanied by a distinctive capacitive behavior as demonstrated by electrochemical measurements. EIS analyses using ATP and L-lysine solutions have shown that protein functionalized films favors the transport of molecular anions with respect to molecular cations. This preference is less pronounced when the concentration of the molecular ions increases. It should be noted that, although all experiments in this work have been conducted using VDAC36, the transport properties of functionalized 3-layered films prepared using the proposed strategy could also be tuned by changing the protein nature. In addition to the usual applications of biomimetic hybrid membranes in fields like nanofluidics and biosensing, the functionalized films engineered in this work

anticipate promising electrode materials for energy storage functions, as for example bio-supercapacitors.

ASSOCIATED CONTENT

Supporting Information. The Supporting Information is available free of charge on the ACS Publications website at DOI: .

Materials and experimental methods. DLS graph and FTIR spectrum of PEDOT NPs, calibration curve for the determination of released CUR.

AUTHOR INFORMATION

Corresponding Authors

* carlos.aleman@upc.edu (C.A.)

ORCID:

Carlos Alemán : 0000-0003-4462-6075

Notes

The authors declare no competing financial interest.

ACKNOWLEDGEMENTS

This work was supported by MINECO (RTI2018-098951-B-I00), the Agència de Gestió d'Ajuts Universitaris i de Recerca (2017SGR359 and FI grant to ML-R) and Consejo Nacional de Ciencia y Tecnología (328467 CVU 621314 to BGM). C.M. and E.A.P. thank the Belgian National Fund for Scientific Research for their research associate and senior research associate positions, respectively. Authors are thanked to Dr. E. Armelin for kind suggestions in EIS experiments.

REFERENCES

1. M. Di Vincenzo, A. Tiraferri, V.-E. Musteata, S. Chisca, R. Sougrat, L.-B. Huang, S. P. Nunes and M. Baroiu, *Nat. Nanotech*., 2020, **16**, 190–196.
2. Y. M. Tu, W. Song, T. Ren, Y. X. Shen, R. Chowdhury, P. Rajapaksha, T. E. Culp, L. Samineni, C. Lang, A. Thokkadam, D. Carson, Y. Dai, A. Mukthar, M. Zhang, A. Parshin, J. N. Sloand, S. H. Medina, M. Grzelakowski, D. Bhattacharya, W. A. Phillip, E. D. Gomez, R. J. Hickey, Y. Wei and M. Kumar, *Nat. Mater*., 2020, **19**, 347–354.
3. M. E. Barbinta-Patrascu, N. Badea, M. Bacalum, C. Ungureanu, I. R. Suica-Bunghez, S. M. Iordache, C. Pirvu, I. Zgura and V. A. Maraloiu, *Mater. Sci. Eng. C*, 2019, **101**, 120–137.
4. A. Puiggalí-Jou, L. J. del Valle and C. Alemán, *Soft Matter*, 2019, **15**, 2722–2736.
5. A. Fuwad, H. Ryu, N. Malmstadt, S. M. Kim and T.-J. Jeon, *Desalination*, 2019, **458**, 97–115.
6. R. Koebnik, K. P. Locher and P. Van Gelder, *Mol. Microbiol.*, 2000, **37**, 239–253.
7. G. M. Grzelakowski, O. Onaca, P. Rigler, M. Kumar and W. Meier, *Small*, 2009, **5**, 2545–2548.
8. W. Meier and C. Nardin, *Angew. Chemie Int. Ed.*, 2000, **39**, 4599–4602.
9. M. M. Pérez-Madrigal, L. J. del Valle, E. Armelin, C. Michaux, G. Roussel, E. A. Perpète and C. Alemán, *ACS Appl. Mater. Interfaces*, 2015, **7**, 1632–1643.

10. A. Puiggalí-Jou, M. M. Pérez-Madrigal, L. J. del Valle, E. Armelin, M. T. Casas, C. Michaux, E. A. Perpète, F. Estrany and C. Alemán, *Nanoscale*, 2016, **8**, 16922–16935.

11. H. X. Gan, H. Zhou, H. J. Lee, Q. Lin and Y. W. Tong, *Langmuir*, 2019, **35**, 7285–7293.

12. X. Zhang, W. Fu, C. G. Palivan and W. Meier, *Sci. Rep.*, 2013, **3**, 2196.

13. H. Wang, T.-S. Chung, Y. W. Tong, K.. Jeyaseelan, A. Armugam, Z. Chen, M. Hong and W. Meier, *Small*, 2012, **8**, 1185–1190.

14. W. Xie, F. He, B. Wang, T.-S. Chung, K. Jeyaseelan, A. Armugam and Y. W. Tong, *J. Mater. Chem. A*, 2013, **1**, 7592–7600.

15. Y. X. Shen, W. C. Song, D. Ryan Barden, T. Ren, C. Lang, H. Feroz, C. B. Henderson, P. O. Saboe, D. Tsai, H. Yan, P. J. Butler, G. C. Bazan, W. A. Phillip, R. J. Hickey III, P. S. Cremer, H. Vashisth and M. Kumar, *Natur. Commun.*, 2018, **9**, 2294.

16. C. Lang, Y. X. Shen, J. A. LaNasa, D. Ye, W. Song, T. J. Zimudzi, M. A. Hickner, E. D. Gomez, E. Winter Gomez, M. Kumar and R. J. Hickey III, *Faraday Discuss.*, 2018, **209**, 179–191.

17. G. Roussel, E. A. Perpète, A. Matagne, E. Tinti and C. Michaux, *Biotechnol. Bioeng.*, 2013, **110**, 417–423.

18. A. Puiggalí-Jou, J. Medina, L. J. del Valle and C. Alemán, *Eur. Polym. J.*, 2016, **75**, 552–564.

19. A. Puiggalí-Jou, J. Pawlowski, L. J. del Valle, C. Michaux, E. A. Perpète, S. Sek and C. Alemán, *ACS Omega*, 2018, **3**, 9003–90019.

20. B. G. Molina, S. Cuesta, H. Besharatloo, J. J. Roa, E. Armelin and C. Aleman, *ACS Appl. Mater. Interfaces*, 2019, **11**, 29427–29435.

21. B. W. Hoogenboom, K. Suda, A. Engel and D. Fotiadis, *J. Mol. Biol.*, 2007, **370**, 246–255.

22. K. Zeth, *Biochim. Biophys. Acta - Bioenerg.*, 2010, **1797**, 1292–1299.

23. E. Blachly-Dyson and M. Forte, *IUBMB Life*, 2001, **52**, 113–118.

24. T. Salinas, S. El Farouk-Ameqrane, E. Ubrig, C. Sauter, A. M. Duchêne and L. Maréchal-Drouard, *Nucleic Acids Res.*, 2014, **42**, 9937–9948.

25. M. Lopes-Rodrigues, A. Matagne, D. Zanuy, C. Alemán, E. A. Perpète and C. Michaux, *Proteins*, 2020, **88**, 729–739.

26. H. Zhang and S. Takeoka, *Macromolecules*, 2012, **45**, 4315–4321.

27. J. Poater, J. Casanovas, M. Solà and C. Alemán, *J. Phys. Chem. A* **2010**, *114*, 1023–1028.

28. R. M. Miller, O. Ces, N. J. Brooks, E. S. J. Robles and J. T. Cabral, *Cryst. Growth Des.*, 2017, **17**, 2428–2437.

29. G. Fabregat, B. Teixeira-Dias, L. J. del Valle, E. Armelin, F. Estrany and C. Alemán, *ACS Appl. Mater. Interfaces*, 2014, **6**, 11940–11954.

30. V. A. Lorenz-Fonfria, *Chem. Rev.* 2020, **120**, 3466–3576.

31. P. J. Y. Paquet, M. A. Diaz, S. Genevrois, M. Grayon, J. M. Verger, X. De Bolle, J. H. Lakey, J. J. Letesson and A. Cloeckaert, *J. Bacteriol.*, 2001, **183**, 4839–4847.

32. D. Kuzum, H. Takano, E. Shim, J. C. Reed, H. Juul, A. G. Richardson, J. de Vries, H. Bink, M. A. Dichter, T. H. Lucas, D. A. Coulter, E. Cubukcu and B. Litt, *Nat. Commun.*, 2014, **5**, 5259.

33. M. Rajesh, C. J. Raj, R. Manikandan, B. C. Kim, S. Y. Park and K. H. A. Yu, *Mater. Today Energy*, 2017, **6**, 96–104.

34. A. D. Aradilla, F. Estrany and C. Alemán, *J. Phys. Chem. C*, 2011, **115**, 8430–8438.

35. N. Phattharasupakun, J. Wutthiprom, S. Kaenket, T. Maihom, J. Limtrakul, M. Probst, S. S. Nagarkar, S. Horike and M. Sawangphruk, *Chem. Commun.*, 2017, **53**, 11786–11789.

36. K. C. Tully, J. F. Whitacre and S. Litster, *J. Power Sources*, 2014, **248**, 348–355.

37. T. Rostovtseva and M. Colombini, *Biophys. J.*, 1997, **72**, 1954–1962.

38. R. Benz, *Biochim. Biophys. Acta*, 1994, **1197**, 167–96.

39. M. Colombini, *Biochim. Biophys. Acta Mol. Cell Res.*, 2016, **1863**, 2498–2502.

40. S. Liu, P. J. Focke, K. Matulef, X. Bian, P. Moënne-Loccoz, F. I. Valiyaveetil and S. W. Lockless, *Proc. Natl. Acad. Sci. USA*, 2015, **112**, 15096–15100.

41. P. K. Devaraneni, A. G. Komarov, C. A. Costantino, J. J. Devereaux, K. Matulef, F. I. Valiyaveetil, *Proc. Natl. Acad. Sci. USA*, 2013, **110**, 15698–15703.

42. A. M. Giudici, M. L. Renart, C. Díaz-García, A. Morales, J. A. Poveda, J. M. González-Ros, *Int. J. Mol. Sci.*, 2019, **20**, 689.

Graphical abstract